AGU PUBLICATIONS

Geochemistry, Geophysics, Geosystems

RESEARCH ARTICLE

10.1002/2013GC005192

Key Points:
- Box model study of Sr isotope ratio evolution in Messinian Mediterranean
- Sr isotope ratios fluctuate in precession cycle during Messinian Salinity Crisis
- Coeval salinity and Sr ratio fluctuations predicted in large range of settings

Correspondence to:
R. P. M. Topper,
r.p.m.topper@uu.nl

Citation:
Topper, R. P. M., S. Lugli, V. Manzi, M. Roveri, and P. Th. Meijer (2014), Precessional control of Sr ratios in marginal basins during the Messinian Salinity Crisis?, *Geochem. Geophys. Geosyst.*, *15*, 1926–1944, doi:10.1002/2013GC005192.

Received 5 DEC 2013
Accepted 16 APR 2014
Accepted article online 21 APR 2014
Published online 29 MAY 2014

Precessional control of Sr ratios in marginal basins during the Messinian Salinity Crisis?

R. P. M. Topper[1], S. Lugli[2], V. Manzi[3,4], M. Roveri[3,4], and P. Th. Meijer[1]

[1]Department of Earth Sciences, Utrecht University, Utrecht, Netherlands, [2]Dipartimento di Scienze della Terra, Universit degli Studi di Modena e Reggio Emilia, Modena, Italy, [3]Dipartimento di Fisica e Scienze della Terra, Università di Parma, Parma, Italy, [4]Alpine Laboratory of Palaeomagnetism, Peveragno, Cuneo, Italy

Abstract Based on $^{87}Sr/^{86}Sr$ data of the Primary Lower Gypsum (PLG) deposits in the Vena del Gesso basin—a marginal basin of the Mediterranean during the Messinian Salinity Crisis—a correlation between $^{87}Sr/^{86}Sr$ values and precessional forcing has recently been proposed but not yet confirmed. In this study, a box model is set up to represent the Miocene Mediterranean deep basin and a connected marginal basin. Measurements of $^{87}Sr/^{86}Sr$ in the Vena del Gesso and estimated salinity extrema are used to constrain model results. In an extensive analysis with this model, we assess whether coeval $^{87}Sr/^{86}Sr$ and salinity fluctuations could have been forced by precession-driven changes in the fresh water budget. A comprehensive set of the controlling parameters is examined to assess the conditions under which precession-driven $^{87}Sr/^{86}Sr$ variations occur and to determine the most likely setting for PLG formation. Model results show that precession-driven $^{87}Sr/^{86}Sr$ and salinity fluctuations in marginal basins are produced in settings within a large range of marginal basin sizes, riverine strontium characteristics, amplitudes of precessional fresh water budget variation, and average fresh water budgets of both the marginal and deep basin. PLG deposition most likely occurred when the Atlantic-Mediterranean connection was restricted, and the average fresh water budget in the Mediterranean was significantly less negative than at present day. Considering the large range of settings in which salinities and $^{87}Sr/^{86}Sr$ fluctuate on a precessional timescale, $^{87}Sr/^{86}Sr$ variations are expected to be a common feature in PLG deposits in marginal basins of the Mediterranean.

1. Introduction

The sedimentary cycles of the Primary Lower Gypsum (PLG; 5.971–5.61 Ma), formed in Mediterranean marginal basins during the first stage of the Messinian Salinity Crisis (MSC; 5.971–5.332 Ma) [*Manzi et al.*, 2013], have long been recognized to be tied to precession-driven climatic changes [*Krijgsman et al.*, 1999; *Hilgen et al.*, 1995]. Recent facies analyses on the shallow water gypsum deposits accumulated during the first MSC stage (PLG) [*Lugli et al.*, 2010] link the different observed facies directly to the precession cycle. This facies-precession correlation allows for bed-to-bed correlation of PLG deposits across the Mediterranean.

Previous work has shown that the combination of strontium isotope ratios ($^{87}Sr/^{86}Sr$) and salinity can be used to constrain the fresh water budget and connectivity of the Mediterranean during the MSC [*Flecker et al.*, 2002; *Topper et al.*, 2011]. The method employed makes use of the fact that there is a pronounced difference in $^{87}Sr/^{86}Sr$ between oceanic and river water. When river discharge constitutes at least 25% of the water fluxes into a basin [*Topper*, 2013], the basinal $^{87}Sr/^{86}Sr$ value will deviate measurably from relatively high oceanic values toward lower riverine values (Table 1).

$^{87}Sr/^{86}Sr$ values have been measured in the PLG of several Mediterranean sections in an attempt to assess the importance of river water in the marginal basins. The most comprehensive records come from the Vena del Gesso basin, the Caltanisetta basin, and the Sorbas basin [*Lugli et al.*, 2007, 2010]. In none of these locations, have large $^{87}Sr/^{86}Sr$ variations been measured in the first five PLG cycles, which are dominated by massive selenite beds. However, from cycle 6 onward, more facies are present in each sedimentary cycle, and a larger variation in $^{87}Sr/^{86}Sr$ values is observed.

The ideal depositional cycle of the PLG, according to *Lugli et al.* [2010], contains the following facies sequence (Figure 1a): bituminous shale (EF1), limestone and dolostone (EF2), giant and massive selenite (EF3), banded selenite (EF4), branching selenite (EF5), displacive selenite (EF6), gypsarenite (EF7), and

© 2014. American Geophysical Union. All Rights Reserved.

Table 1. Overview of Parameter Values Used to Set Up the Model

Parameter	Detail	Value	Reference
Mediterranean Volume/Surface Area			
V	Late Miocene volume	3750.7×10^{12} m^3	*Meijer et al.* [2004]
A	Late Miocene surface area	2.4780×10^{12} m^2	*Meijer et al.* [2004]
Messinian Fresh Water Fluxes			
E-P	Evaporation-precipitation	1 m yr^{-1}	*Gladstone et al.* [2007]
R_{west}	River input in WMed	5526.4 m^3 s^{-1}	*Gladstone et al.* [2007]
R_{east}	River input in EMed	36067.4 m^3 s^{-1}	*Gladstone et al.* [2007]
R_{Chad}	Chad basin discharge	66545.0 m^3 s^{-1}	*Gladstone et al.* [2007]
Salinity			
S_A	Ocean water	35 kg m^{-3}	
S_R	River input	0 kg m^{-3}	
Gypsum ($CaSO_4$)			
G_A	Ocean water	1.27 kg m^{-3}	*Leeder* [1999]
G_R	River input	0 kg m^{-3}	
G_{SAT}	Gypsum saturation	5.25 kg m^{-3}	
Halite (NaCl)			
H_A	Ocean water	27.21 kg m^{-3}	*Leeder* [1999]
H_R	River input	0 kg m^{-3}	
H_{SAT}	Halite saturation	272.1 kg m^{-3}	
Strontium Concentration			
$[Sr]_A$	Ocean water	8×10^{-3} kg m^{-3}	*Palmer and Edmond* [1989]
$[Sr]_{Nile}$	Nile water	0.235×10^{-3} kg m^{-3}	*Brass* [1976]
$[Sr]_{Rhone}$	Rhone water	0.520×10^{-3} kg m^{-3}	*Albarède and Michard* [1987]
$[Sr]_R$	Average Rhone and Nile water	0.3×10^{-3} kg m^{-3}	*Flecker et al.* [2002]
Strontium Isotope Ratios			
$^{87}Sr/^{86}Sr_A$	Average during MSC	0.709006	*McArthur et al.* [2001]
$^{87}Sr/^{86}Sr_{Mesozoic}$	Mesozoic ocean water	0.7068–0.7084	*McArthur et al.* [2001]
$^{87}Sr/^{86}Sr_{Hydrothermal}$	Hydrothermal activity	~0.703	*Palmer and Edmond* [1989]
$^{87}Sr/^{86}Sr_{River}$	Global average river water	0.7119	*Palmer and Edmond* [1989]
$^{87}Sr/^{86}Sr_{Nile}$	Nile water	0.7060	*Brass* [1976]
$^{87}Sr/^{86}Sr_{Rhone}$	Rhone water	0.708719	*Albarède and Michard* [1987]
$^{87}Sr/^{86}Sr_R$	Average Rhone and Nile water	0.707427	*Flecker et al.* [2002]

gypsrudite (EF8); facies EF6 (displacive selenite) is actually a postdepositional feature and will not be considered in this paper. Whether all these facies are formed depends on the position, particularly the water depth, in the marginal basin. In deeper parts of a basin, the pycnocline will always be far from the bottom and only shale and massive selenite form. In shallower parts, fluctuations of the depth of the pycnocline affect the facies formed, e.g., massive selenite forms when the pycnocline is away from the bottom, banded selenite when the pycnocline is close to the bottom, and branching selenite during a phase of shallowing pycnocline depth [*Lugli et al.*, 2010, Figure 9]. In a depositional cycle, the different facies and variations in salt concentrations and $^{87}Sr/^{86}Sr$ are proposed to be correlatable with the changing fresh water budget during a precessional cycle as illustrated in Figure 1a.

In this hypothesis, river input is relatively high and evaporation-precipitation (E-P) low in a precession minimum, resulting in basin-wide undersaturation of evaporites and deposition of shales (EF1). In restricted marginal basins, due to a relatively high river input with respect to input from the deep Mediterranean, $^{87}Sr/^{86}Sr$ values are expected to deviate from oceanic values toward lower riverine values. Moving from the precession minimum to the precession maximum, river input decreases while E-P increases. Within a prolonged period with a negative fresh water budget, the increasing salt concentration will at some point result in the deposition of facies EF2–EF4. The $^{87}Sr/^{86}Sr$ values are expected to move from the low $^{87}Sr/^{86}Sr$ values of the precession minimum to higher values associated with the increased importance of inflow from the deep basin in the marginal basin water budget. Facies EF5–EF8 are consecutively formed when the peak evaporative conditions have passed. River input and its low $^{87}Sr/^{86}Sr$ signature become progressively more dominant again when approaching the precession minimum.

Unfortunately, because of, as yet, insufficient sampling resolution (i.e., one sample per facies was measured) and data from only three sites, the link between measured variations in $^{87}Sr/^{86}Sr$ values and the precessional cycle in Mediterranean marginal basins remains tentative. One way forward would be high-resolution

© 2014. American Geophysical Union. All Rights Reserved.

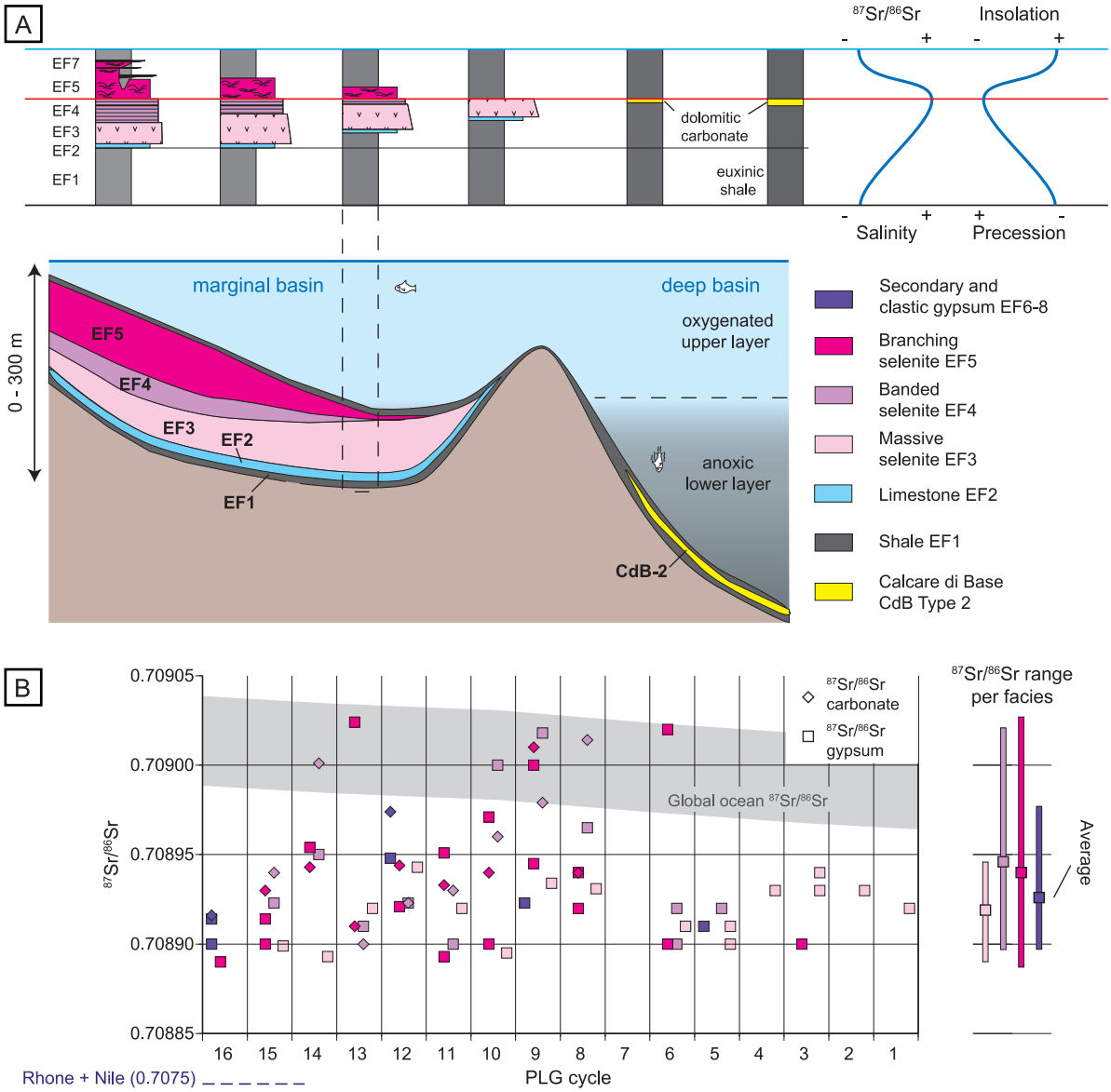

Figure 1. (a) Schematic overview of lateral facies transitions within a marginal and deep basin, and the corresponding depositional sequences formed during a precession cycle (modified after *Lugli et al*. [2010]). Also shown is the correlation between the precession signal and the changing facies, salinity and $^{87}Sr/^{86}Sr$ as proposed by *Lugli et al*. [2010]. (b) An overview of the $^{87}Sr/^{86}Sr$ data set from the Vena del Gesso, Italy. The $^{87}Sr/^{86}Sr$ data are sorted by facies, not relative or absolute age, in each PLG cycle. The $^{87}Sr/^{86}Sr$ ranges and average $^{87}Sr/^{86}Sr$ of each facies have been calculated from all data, i.e., $^{87}Sr/^{86}Sr$ measured in both carbonate and gypsum.

sampling of multiple PLG sections throughout the Mediterranean. A complementary approach, which we will pursue in this study, is to use a simple box model to examine whether precession induced water budget variations can cause $^{87}Sr/^{86}Sr$ values to fluctuate in marginal basins during PLG formation. Because it is not certain whether precession-driven climate change can explain $^{87}Sr/^{86}Sr$ variations, we first look, as a proof of concept, for a single model setup where $^{87}Sr/^{86}Sr$ variations are produced in a generic marginal basin when forced by a precessional signal. Besides fluctuations in $^{87}Sr/^{86}Sr$, the results will have to reproduce the varying salt concentrations implied by the changing facies within a PLG cycle, which we will explain in section 2. Once a proof of concept is demonstrated, we will examine, in section 4, a large range of parameters to identify their influence on the modeled cyclicity; these parameters are basin size, river water characteristics (Sr concentration and ratio), connectivity of the marginal basin with the deep Mediterranean and of the Mediterranean and Atlantic, the average fresh water budget, and the amplitude of the variation of the fresh water budget during a precession cycle. Ultimately, this will allow us to assess the likelihood of precession

© 2014. American Geophysical Union. All Rights Reserved.

induced $^{87}Sr/^{86}Sr$ variations, constrain the setting in which $^{87}Sr/^{86}Sr$ values are precession controlled and PLG formation takes place, and establish a context for existing and new $^{87}Sr/^{86}Sr$ data.

2. Observational Constraints

The facies sequence of a single PLG cycle indicates the basin underwent large salinity changes in a relatively short time. Fish remains, foraminifera, insects, leaves, and twig remains in the organic-rich laminated shale layers in several Italian sections (Vena del Gesso, Piedmont Basin, and Sicily) are indicators of continental water fluxes periodically diluting the evaporite basin [*Lugli et al*., 2010, and references therein]. For fish and foraminifera to survive, salinities at that time must have been marine or even brackish. To constrain the model results, we accept all results where the minimum salinity at some time during a precession cycle is lower than 50 g/L. Although redundant, we also check that gypsum deposition in the marginal basin does not continue throughout the whole precession cycle.

With the minimum salinity established, the maximum salinity is another constraint on the model results. Gypsum is observed in every cycle of the PLG in at least one facies. Therefore, gypsum saturation must be reached in part of the cycle in the marginal basin. The absence of halite in both marginal and deep basins during the first MSC phase implies that halite saturation is the upper limit on salinity during PLG formation (in the sense of *Roveri et al*. [2008] and *CIESM* [2008]).

Lugli et al. [2010] point out that $^{87}Sr/^{86}Sr$ values vary within a depositional cycle, with generally higher values in the middle part of a cycle and lower values in the lower and upper parts where ratios near 0.70890 were explained by a relatively high fresh water input. The relation between facies and $^{87}Sr/^{86}Sr$ is not unambiguous in all cycles of the highest resolution (Vena del Gesso basin) data set (Figure 1b). The spread and averages of EF4 and EF5 $^{87}Sr/^{86}Sr$ measurements are, respectively, larger and slightly higher than those in EF3 and EF6, but low $^{87}Sr/^{86}Sr$ values are also found in EF4 and EF5. Noteworthy is that the majority ($\approx$ 80%) of the $^{87}Sr/^{86}Sr$ data and all facies-averaged values are in the relatively small range 0.70890–0.70895 with outliers closer to oceanic values. Additional new data are needed to conclusively confirm or refute the existence of a correlation between the different gypsum facies and $^{87}Sr/^{86}Sr$ values.

Moreover, only part of the range of $^{87}Sr/^{86}Sr$ variation in a precession cycle is sampled because strontium ratios in the PLG deposits can only be measured in evaporite facies, i.e., carbonates and gypsum. These facies are expected to have formed when $E\text{-}P > R$, and consequently $^{87}Sr/^{86}Sr$ in marginal basins was most strongly affected by oceanic inflow. The measured ratios in the evaporites therefore represent the upper part of the $^{87}Sr/^{86}Sr$ range in a precession cycle. $87Sr/^{86}Sr$ minima will occur when river input is dominant, salinities are low, and shales are deposited.

Since the available $^{87}Sr/^{86}Sr$ measurements on PLG deposits are mainly from the Vena del Gesso Basin, we will use those measurements to constrain the model results. Because $^{87}Sr/^{86}Sr$ values during shale deposition are expected to be lower than any value measured in the gypsum, model results will be constrained such that the maximum $^{87}Sr/^{86}Sr$ in a precession cycle should be at least the lowest $^{87}Sr/^{86}Sr$ value of the gypsum (0.70890), and the minimum $^{87}Sr/^{86}Sr$ should be at most 0.70890.

3. Model Description and Experimental Design

The model used in this study is based on the box model used and described in *Topper et al*. [2011]. In this model, a set of coupled ordinary differential equations, i.e., a set of full nonsteady state equations, is solved using the second-order Runge-Kutta method with adaptive time stepping (for more information about the model, see *Topper et al*. [2011]). As shown in *Topper and Meijer* [2013], the sill near Sicily was most likely not restrictive during the Messinian, keeping water characteristics in the western and eastern Mediterranean basins at similar values. Therefore, for the present purpose, the Mediterranean can be represented with only two boxes, one for the deep basins of both the eastern and western Mediterranean, and one for a marginal basin (Figure 2a). Although more than one marginal basin existed during the MSC, their combined volume is small compared to that of the deep basins and their combined impact on the water characteristics of the deep basin is negligible. Therefore, all marginal basins, but one, are included in the deep basin box. The single marginal basin allows to examine the generic behavior of a marginal basin connected to the deep basins.

© 2014. American Geophysical Union. All Rights Reserved.

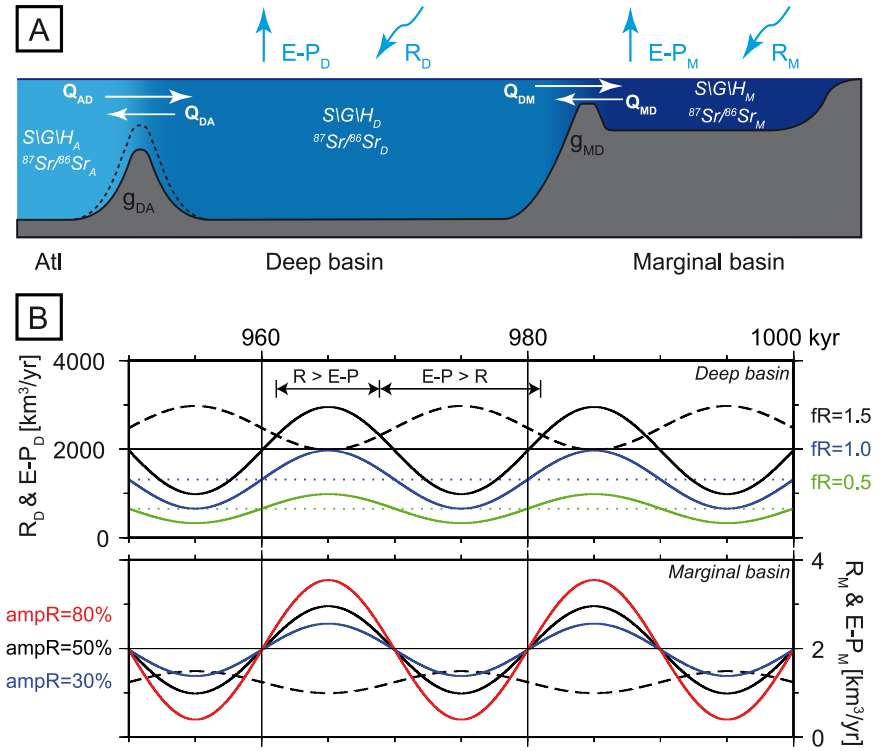

Figure 2. (a) Graphic representation of the box model. White arrows indicate volume fluxes (Qs) between the basins; the first subscript character represents the source, the second one the destination. The fresh water budget consists of E-P_D and E-P_M, evaporation minus precipitation, and R_D and R_M, river discharges. S(alinity)\G(ypsum concentration)\H(alite concentration)$_x$ and $^{87}Sr/^{86}Sr_x$ are the water characteristics of the respective basins (indicated by *x*). (b) Fresh water forcings, R (solid line) and E-P (dashed line), for the deep basin (top) and marginal basin (bottom) during 2.5 precession cycles (50 kyr, ending at the model run time of 1 Myr). The effect of a change in *fR* on the river discharge is demonstrated in the top where dotted lines indicate the precession-averaged river discharge. The effect of *ampR* is demonstrated in the bottom.

The deep basin box is connected to an infinite volume of water with constant water characteristics representing the Atlantic. Water exchange between the boxes consists of (1) a deep flow which is linearly proportional to the density difference between the boxes and (2) a surface flow which compensates for outflow and the fresh water deficit, i.e., evaporation-precipitation-river discharge (E-P-R), to keep the volume in each of the boxes constant. The density difference between the boxes is only a function of salinity, i.e., temperature differences are neglected following *Topper et al.* [2011]. Proportionality factors g_{DA} (deep basin-Atlantic connection) and g_{MD} (marginal basin-deep basin connection) relate the density difference between the two corresponding boxes to an outflow. The present-day Strait of Gibraltar can be represented with a factor of $\approx 10^5$ m^3 s^{-1} (g L^{-1})$^{-1}$ and a gateway near closure with 10^0 (bulky units of factors will be omitted from here onward).

The fresh water budget in the model consists of an average river discharge and E-P on which a sinusoidal variation is superposed to represent changes during a precession cycle (Figure 2b). Inherent to this representation of precessional water budget variation, are the assumptions that (1) river discharge and evaporation-precipitation variations are in phase with the precession signal and (2) the variation is proportional to the strength of the precession signal. Both assumptions are corroborated by the results of climate model studies [*Kutzbach et al.*, 2008; *Tuenter et al.*, 2005; *Weber and Tuenter*, 2011]. The Late Miocene fresh water budget is derived from the results from *Gladstone et al.* [2007] where we leave out the contribution from the Chad basin following *Topper et al.* [2011]. Evaporation minus precipitation is 1 m/yr, and the total river discharge (R) into the Mediterranean is 41.6×10^3 m^3 s^{-1} (Table 1). With respect to present-day values (E-P = 0.6 m/yr and R = 17.7×10^3 m^3 s^{-1} [*Mariotti et al.*, 2002; *Meijer and Krijgsman*, 2005]), both E-P and R are higher in the Late Miocene water budget. The fresh water deficit (E-P-R), however, is similar at 0.5 m/yr. A more detailed description of the water budget can be found in *Topper et al.* [2011].

While the average E-P is constant at 1 m/yr in all model runs and the same over deep and marginal basins, the amount of river discharge which flows in the deep and marginal basin will be varied by multiplying the

© 2014. American Geophysical Union. All Rights Reserved.

reference Late Miocene river discharge with the factors fR_D and fR_M, respectively. The amplitude of the sinusoidal variation in river discharge (*ampR*) and E-P (*ampE*) is expressed as a percentage of the average river discharge and is hence dependent on the *fR* factors. When the average river discharge is shifted by the *fR*s, the absolute amplitude of variation during a precession cycle also changes (Figure 2b). The sinusoidal variations have a period of 20 kyr, i.e., an idealized length in between the two dominant precession frequencies (19–23 kyr). All results presented are derived from the last 2.5 precession cycles (50 kyr) of each 1 Myr model run. At this time, a dynamic equilibrium has been reached, i.e., minimum and maximum values of water characteristics are constant in consecutive precession cycles.

In both the marginal basin box and the deep basin box, the model solves for strontium concentration, $^{87}Sr/^{86}Sr$, total salinity, and gypsum ($CaSO_4$) and halite (NaCl) concentrations. If gypsum and/or halite concentrations exceed their respective saturation concentrations (Table 1), all gypsum/halite in excess of saturation is deposited. The algorithms for gypsum and halite concentration and deposition are presented in more detail in *Topper and Meijer* [2013]. Neither dissolution of evaporites nor incorporation of Sr in the precipitating evaporites is taken into account in our model. Because quantitative constraints on both processes are lacking, their incorporation in the model would only add further complexity and uncertainty to the model results.

Although *Topper and Meijer* [2013] included a parametrization of water column stratification in their model, the unknown behavior and distribution of strontium in a stratified basin prohibits its use here. Water properties in each basin are therefore homogeneous. In contrast, PLG is bottom-grown and the facies indicate deposition in a well-stratified shallow ($<$300 m) marginal basin with a fluctuating depth of the pycnocline. In *Lugli et al*. [2010], the fluctuations in the depth of the pycnocline are used interchangeably with sea level variations during a depositional cycle. However, the cause of sea level variations during a precession cycle is unclear. We, therefore, assume that sea level was constant and only the depth of the pycnocline fluctuated. Gypsum precipitation from a dense bottom layer (below the pycnocline) is expected to commence before the whole basin reaches gypsum saturation. Depending on the thickness of the bottom layer, which is supposedly different during formation of the different gypsum facies, and the degree of undersaturation in the surface layer, gypsum precipitation from the bottom layer will start when the basin-averaged salinity is at 75–100% of gypsum saturation. Therefore, when checking results for the constraints on maximum gypsum and halite concentrations, values $>$90% of the respective saturation value will be considered as having reached saturation. Results are not significantly affected by the choice of another percentage.

Also related to the lack of stratification in the model is the assumption that Sr ratios measured in bottom-grown evaporites are representative for the whole basin. The presence of yearly cycles in gypsum and halite deposits on Sicily [*Manzi et al*., 2012], formed in the MSC phase after the PLG, implies that mixing of the whole water column, or at least dense water formation from the surface layer, occurred at least once a year. Because we are interested in precessional time scales, such yearly mixing, if also active during PLG formation, would justify the assumption of constant $^{87}Sr/^{86}Sr$ in a marginal basin over longer time scales.

Constant in all of the model runs are the salt concentrations and Sr ratio in the Atlantic, also used as initial conditions in all boxes, and the combined volume of the marginal and deep Mediterranean basin (Table 1). Boundary conditions that can be varied between experiments are (1) the size (volume and surface area) of the marginal basin as a percentage of the total Mediterranean volume and surface area, (2) the riverine $^{87}Sr/^{86}Sr$ and Sr concentration, (3) the amount of river discharge in the marginal basin as a percentage of the total Mediterranean river input, (4) the average river discharge during a precession cycle, (5) the amplitude of the variation in the fresh water budget during a precession cycle, (6) the size of the connection between the deep Mediterranean and the Atlantic, and (7) the size of the connection between the deep and marginal basin.

Boundary conditions (5)–(7) are the main parameters to be examined in this study and are varied between the model runs. Values for boundary conditions (1)–(4) are prescribed in the default model setup:

1. A marginal basin with a surface area of 0.05% and a volume of 0.01% of the total Mediterranean surface area and volume ($\approx 30 \times 40$ km, 375 km^3). This results in an average depth of 300 m in the marginal basin. This marginal basin size is a reasonable first-order estimate for the Vena del Gesso, Sorbas, and Sicilian wedge-top basins.

2. The riverine $^{87}Sr/^{86}Sr$ is 0.7075, and the Sr concentration is 150×10^{-6} kg/m^3.

3. Of the total Mediterranean river input, 0.1% flows into the marginal basin.

© 2014. American Geophysical Union. All Rights Reserved.

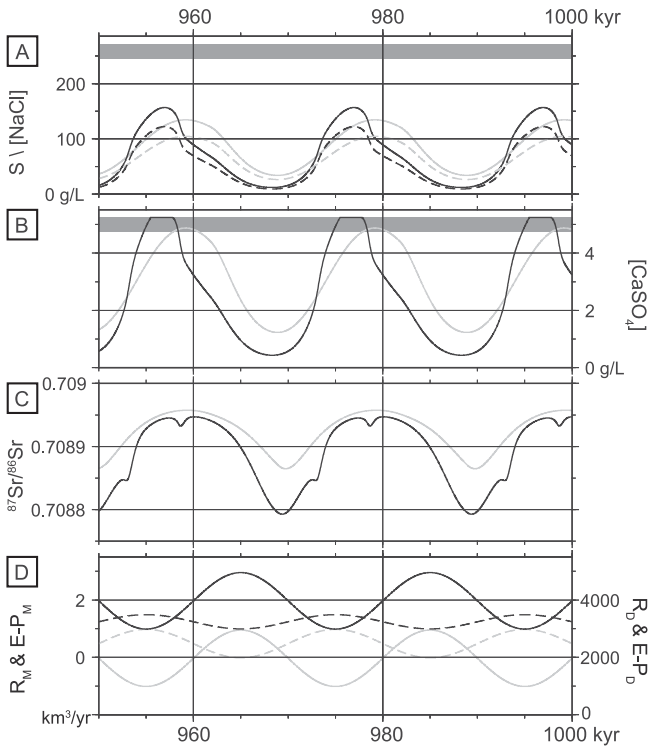

Figure 3. Evolution of water characteristics in the last 50 kyr of a 1 Myr model run. Shown are for the deep basin (gray) and marginal basin (black): (a) salinity (solid line) and NaCl concentration (dashed line), (b) $CaSO_4$ concentration, (c) $^{87}Sr/^{86}Sr$, and (d) R (solid line) and E-P (dashed line). Gray bars in Figures 3a and 3b indicate the range of respectively >90% halite and gypsum saturation.

4. The precession-averaged river discharge is 1.5 times, i.e., $fR = 1.5$, the Late Miocene river input of *Gladstone et al.* [2007]. Other model studies have shown that Messinian Sr data and observed evaporite thicknesses can be reproduced with a model set up with this fresh water budget [*Topper et al.*, 2011; *Topper and Meijer*, 2013].

The sensitivity of the results to these choices will be discussed in section 4.3.

4. Results and Analysis

4.1. Proof of Concept

As a proof of concept, Figure 3 shows the results of a model setup that satisfies all observational constraints. The default setup, explained above, has been combined with a restricted connection between the Atlantic and the deep basin ($g_{DA} = 10^2$), an even more restricted connection between the deep and marginal basins ($g_{MD} = 10^0$), $ampR = 50\%$ and $ampE = 20\%$.

As long as neither basin is saturated for halite, halite concentrations follow the total salt concentrations, as visible Figure 3a. Noteworthy are the distinct shapes of the curves for the deep and marginal basin: the curves from the deep basin are smooth and regular, and the marginal basin curves change faster and have irregular shapes. This difference reflects the greater sensitivity of the marginal basin to changes in the fresh water budget and interbasinal exchange. The rate of change of the water characteristics in a marginal basin with a small volume is generally higher than that of the large deep basin. Even though the exchange fluxes and the fresh water budget of the marginal basin are smaller, the volume of those fluxes in relation to the basin volume is higher and consequently has a larger impact on the water characteristics.

Focusing on salinity variation in the deep basin, peak salinities, minimum and maximum, are reached close to the time where the water budget switches sign. As long as E-P > R in the deep basin (gray lines in Figure 3d), the fresh water budget is negative and salinities increase. As soon as the fresh water budget switches to positive (intersection of E-P and R curves in Figure 3d), river input is dominant (R > E-P) and salinities drop continuously until the fresh water budget switches sign again. The intervals with E-P > R and R > E-P have different lengths because the precession-averaged E-P exceeds R in the deep basin. The switches in water budget do not precisely coincide with the salinity peaks in the deep basin due to the interaction with the marginal basin. In the marginal basin, the switches in the sign of the water budget occur at different times because on average R > E-P. Besides the relative size of the precession-averaged E-P and R, *ampR* and *ampE* also affect the duration of the intervals with positive and negative fresh water budget as shown in Figure 2b. The observant reader will have noticed that peaks in salinity, and hence gypsum concentration, do not coincide with the peaks in the precession signal. A more detailed discussion of this offset and its implication for cyclostratigraphy during the MSC are beyond the scope of this paper and can be found in R. P. M. Topper and P. Th. Meijer, The precessional phase lag of Messinian gypsum deposition in Mediterranean marginal basins, submitted to *Palaeogeography, Palaeoclimatology, Palaeoecology* (2014).

© 2014. American Geophysical Union. All Rights Reserved.

While halite concentration is never close to saturation, and hence complies with the observational constraint, gypsum saturation is reached in the marginal basin and its concentration is close to saturation in the deep basin (Figure 3b). The interval with gypsum deposition has a duration of only 3680 year, not even 20% of the length of the precession cycle. This duration is strongly dependent on the average fresh water budget and its amplitudes of variation and the size of the connection to the deep basin. A more detailed examination of the duration of gypsum deposition will follow in section 4.4.

Although the $^{87}Sr/^{86}Sr$ curve for the deep basin is smooth and regular, $^{87}Sr/^{86}Sr$ in the marginal basin exhibits multiple irregularities (Figure 3c). The small bumps and slope changes in the curve coincide with changes in the exchange with the deep basin, in turn forced by a changing fresh water budget. Shortly after salinities peak at 957 kyr, the marginal basin switches to a positive fresh water budget ($R > E\text{-}P$, intersection of the curves in Figure 3d) and salinity and $^{87}Sr/^{86}Sr$ drop sharply. When the marginal basin salinity drops below its coeval deep basin value at 959.5 kyr, exchange between the two basins switches direction: more saline water from the deep basin enters the marginal basin at depth while outflow occurs at the surface. For a short while, the deep basin inflow is able to oppose the increasing inflow of low $^{87}Sr/^{86}Sr$ river water and $^{87}Sr/^{86}Sr$ rises a little, until $R \gg E\text{-}P$ at 960 kyr and $^{87}Sr/^{86}Sr$ drops to riverine values. At the switch back to a negative fresh water budget, the opposite takes place. 87Sr/^{86}Sr is already rising since 969.4 kyr due to an inflow from the deep basin driven by the relatively large salinity difference between the basins and a decreasing river input. After the switch to a negative water budget at 972 kyr, marginal basin salinity increases to the deep basinal value. At equal salinities, the exchange between the basins slows to a halt, and river discharge is shortly the only source of $^{87}Sr/^{86}Sr$ at 973 kyr, until $E\text{-}P \gg R$ and deep basin inflow overwhelms the river signal again.

Within this complex system, high $^{87}Sr/^{86}Sr$ always coincides with the high salinities and low $^{87}Sr/^{86}Sr$ with low salinities. Furthermore, the model affirms that precession-driven climatic changes can explain coeval variations in $^{87}Sr/^{86}Sr$ and salinity in a way that is consistent with all observational constraints. It should be noted that the range of $^{87}Sr/^{86}Sr$ ratios within the interval of evaporite formation is relatively small compared to the range within the whole precession cycle.

4.2. The Full Parameter Range

Since we have demonstrated that a scenario exists that fits all constraints, a broader range of parameters must now be examined to assess the range of parameters giving rise to precession-driven fluctuations of $^{87}Sr/^{86}Sr$ and salinity and to gain insight in the controlling factors. While retaining the default setup, the size of the two gateways, and *ampR* and *ampE* are varied in different combinations, resulting in 61.812 model runs. Because the observational constraints are only on the minimum and maximum values reached within a precessional cycle, each model run can be checked for compliance with the constraints with only those values. Thus, the minimum and maximum values of salinity, gypsum concentration, halite concentration, and $^{87}Sr/^{86}Sr$ have been monitored in the last 50 kyr of each 1 Myr run and are shown in Figures 4a–4h.

The subfigures in Figure 4 are comprised of 4×3 frames with marginal basin results and 1×3 frames with the results of the deep basin. Each marginal basin frame corresponds to a different combination of g_{DA} and g_{MD}, as explained in Figure 4i. Results for the deep basin are not visibly affected by g_{MD} and are hence only shown for different g_{DA}. Moving from the bottom to the top row in a subfigure such as Figure 4a (from $g_{DA} = 10^2$ to $g_{DA} = 10^0$), the size of the Atlantic-Mediterranean connection shrinks; going from the first to the fourth column (from $g_{MD} = 10^{-2}$ to $g_{MD} = 10^4$), the size of the deep-marginal basin connection increases. Along the horizontal axis of every single frame, *ampE* is varied between 0 and 50% while *ampR* varies along every vertical axis between 0 and 100% (Figure 4j). Shading is used to emphasize those results that comply with the constraint on the shown variable in the corresponding basin. For example, the range of *ampR* and *ampE* where the minimum salinity <50 g/L is shaded in each marginal basin frame of Figure 4a. The minimum and maximum values from Figure 3 are indicated in each subfigure with white stars.

Before we focus on the results of the marginal basin, understanding the general behavior of the deep basin is necessary. The volume of the marginal basin is only 0.01% of the total Mediterranean volume. Hence, even dramatic changes in the water characteristics of the marginal basin have little impact on the deep basin. Therefore, increasing the size of the connection between the marginal and deep basin, which allows for a larger exchange between the basins, does not change the minima/maxima of the deep basin. Reducing the connection with the Atlantic, on the other hand, does affect the water characteristics of the deep

© 2014. American Geophysical Union. All Rights Reserved.

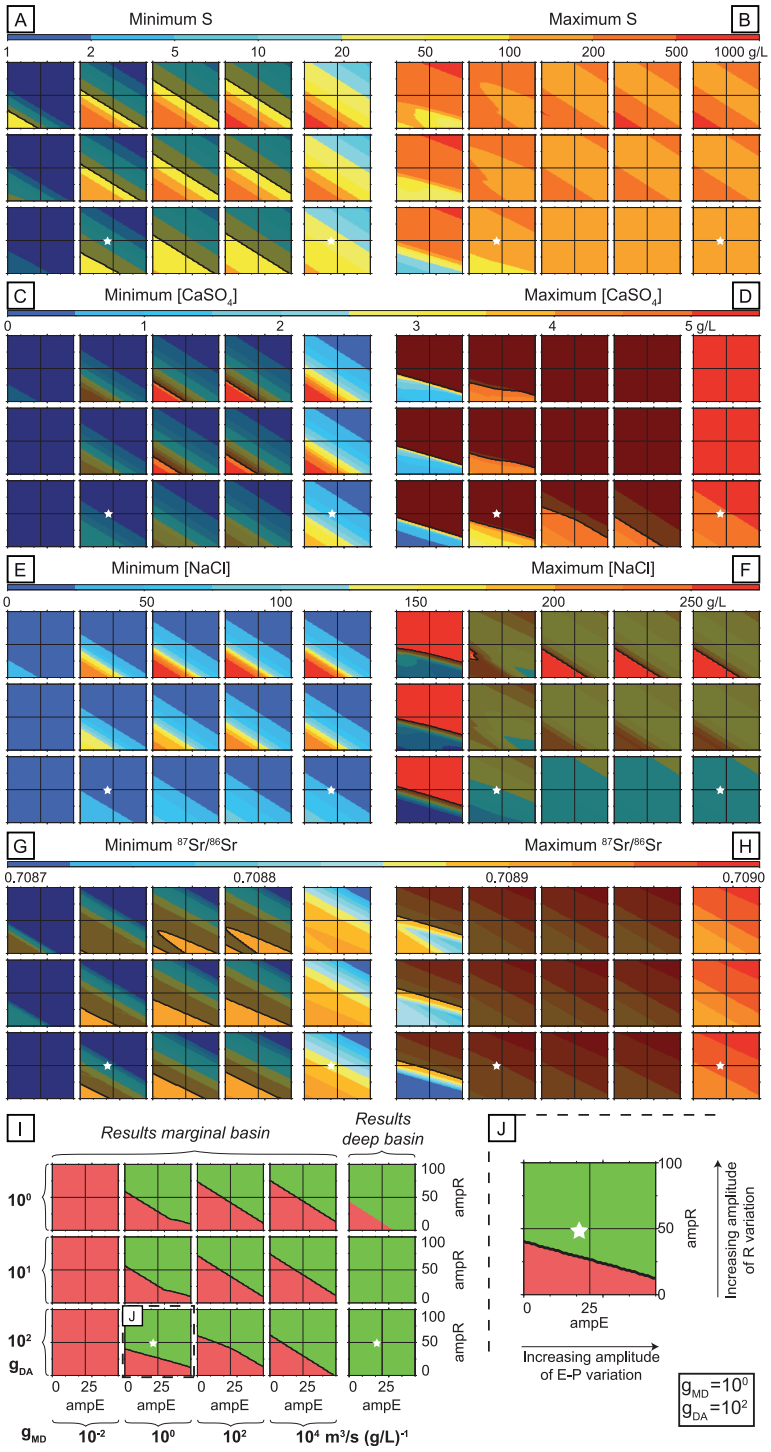

Figure 4. (a–h) Composed of 4 × 3 frames for the marginal basin results and 1 × 3 frames for the deep basin results. Figures 4i and 4j illustrate how to read these frames. Minimum and maximum (a, b) salinity, (c, d) gypsum concentration, (e, f) halite concentration, and (g, h) $^{87}Sr/^{86}Sr$ in a single precessional cycle. In Figure 4a, the area where the salinity minimum in the marginal basin is <50 g/L is shaded. The shaded segment is also delimited by a thick black line. In Figure 4c, the area where the minimum gypsum concentration in the marginal basin is <90% of the saturation value is shaded. In Figure 4d, the area where the maximum gypsum concentration is >90% of the saturation value is shaded. In Figure 4f, the area where the maximum halite concentration is <90% of the saturation value is shaded. In Figure 4g, the area where the minimum $^{87}Sr/^{86}Sr < 0.7089$ in the marginal basin is shaded. In Figure 4h, the area where the maximum $^{87}Sr/^{86}Sr > 0.7089$ is shaded. Shown in Figure 4i is where the deep and marginal basin characteristics meet all the constraints (green) or not (red). In the areas above the thick black lines, constraints in both the deep and marginal basin are met, i.e., these areas contain the scenarios that fit all observations for the PLG phase. The minimum and maximum values from Figure 3 are indicated with the white stars in each subfigure.

© 2014. American Geophysical Union. All Rights Reserved.

basin. With a nonzero fresh water deficit, water characteristics can deviate further from Atlantic values when the connection is smaller. Consequently, salinity, gypsum, and halite minima and maxima are higher while $^{87}Sr/^{86}Sr$ minima and maxima are lower (Figures 4a–4h; compare frames at different values of g_{DA}).

The influence of *ampR* and *ampE* can be examined within a single frame, i.e., constant g_{DA}. Concentration minima (S, [$CaSO_4$], and [NaCl]; Figures 4a, 4c, and 4e) decrease when *ampR* increases at constant *ampE*. When *ampR* increases, concentration is affected in two ways: (1) the time interval where R > E-P becomes longer, i.e., the precession-averaged concentration drops, and (2) the fresh water excess (R-E-P) in a precession minimum becomes increasingly larger at higher *ampR*, i.e., the deviation from the average increases (Figure 2b). Increasing *ampE* at constant *ampR* affects the concentration minima in a similar fashion; (1) the time interval where E-P > R becomes longer and (2) the fresh water deficit (E-P-R) in a precession minimum becomes increasingly more negative. Increasing both *ampR* and *ampE* enhances their individual influence, leading to lower concentration minima at higher amplitudes of variation.

$^{87}Sr/^{86}Sr$ minima are affected in a similar fashion, and ratios drop toward higher *ampR* and *ampE* (Figure 4g). However, at $g_{DA} = 10^0$, a small area at low *ampR* and *ampE* deviates from this pattern. This parameter range has a negative fresh water budget in the deep basin throughout the precession cycle which leads to aberrant behavior of $^{87}Sr/^{86}Sr$, whereas it is not visible in the concentration minima.

When *ampR* and *ampE* increase, concentration maxima (Figures 4b, 4d, and 4f) change in a way different from the concentration minima. Toward higher amplitudes, the increasing duration of the time interval with R > E-P and the increasing deviation from the average, i.e., larger difference between minima and maxima, do not enhance each others. Along a line from low to high amplitude variation of R and/or E-P, e.g., bottom left to top right corner of a single frame, concentration maxima decrease before they increase again. At first, the lengthening interval with R > E-P lowers the precession-averaged concentration faster than the increasing deviation from the average can compensate for. Then, at higher amplitudes, the duration of the interval with R > E-P stabilizes and the increasing deviation from the precessional average causes the maxima to rise again. The effect of these two competing processes is not visible in $CaSO_4$ maxima because these do not rise beyond saturation.

Once again, $^{87}Sr/^{86}Sr$ maxima show a different pattern (Figure 4h). Where concentration maxima drop, $^{87}Sr/^{86}Sr$ maxima steadily rise. When the precession-averaged Sr concentration decreases because of higher *ampR* and *ampE*, the buffering action of the Mediterranean decreases. Consequently, the impact of an inflow of water with a $^{87}Sr/^{86}Sr$ deviating from the deep basin $^{87}Sr/^{86}Sr$, i.e., Atlantic inflow or river discharge, becomes larger and the amplitude of $^{87}Sr/^{86}Sr$ variations increases with increasing *ampR* and *ampE*.

Concentrations and $^{87}Sr/^{86}Sr$ in the marginal basin are largely similar to those in the deep basin when their connection is relatively large ($g_{MD} \geq 10^2$), i.e., the interbasinal exchange evens out all differences. With a smaller gateway ($g_{MD} \leq 10^0$), and hence less exchange, the marginal basin values deviate from the deep basin values: minima are generally lower and maxima higher. Because the marginal basin gets twice the amount of river input per unit surface area compared to the deep basin, $^{87}Sr/^{86}Sr$ in the marginal basin is always slightly lower than in the deep basin. Moreover, the higher river input causes a positive water budget to persist during a whole precession cycle when *ampR* is low. The range of amplitudes with a constant positive water budget in the marginal basin is clearly discernible in the low $CaSO_4$, NaCl, and $^{87}Sr/^{86}Sr$ maxima of the marginal basin when the connection with the deep basin is severely restricted ($g_{MD} = 10^{-2}$; Figures 4d, 4f, and 4h).

From the observational constraints outlined in section 2, only one relates to the deep basin: halite saturation should not be reached anytime during a precession cycle. This constraint is easily met when the connection between the Atlantic and Mediterranean is relatively large ($g_{DA} \geq 10^1$). Only when the connection to the Atlantic is severely restricted, halite saturation is reached at low *ampR* and *ampE*. The parameter range that complies with this constraint is colored green in Figure 4i in the fifth column. In the left four columns, the green parameter range above the black lines complies with all constraints on the marginal basin results. Hence, the constraint on the deep basin results is never a limiting factor.

A restricted marginal basin ($g_{MD} \leq 10^2$) connected to a slightly restricted deep basin ($g_{DA} \leq 10^2$) is advantageous for reaching a lower than marine salinity, interruption of gypsum deposition, and $^{87}Sr/^{86}Sr < 0.7089$ in the marginal basin at low amplitude variations. Of these three, the low salinity constraint curtails the

© 2014. American Geophysical Union. All Rights Reserved.

parameter range that complies with the constraints the most. A marginal basin reaches gypsum saturation and $^{87}Sr/^{86}Sr > 0.7089$ when the deep basin does, unless the marginal basin is severely restricted ($g_{MD} = 10^{-2}$) in combination with an unceasing fresh water excess. At $g_{MD} = 10^{-2}$, in the marginal basin either gypsum saturation is not reached or halite saturation is reached. As such, this setting never complies with all constraints and is therefore an unlikely setting for the PLG stage. In all other settings, the constraints on the salinity minimum and the gypsum maximum exclude only a part of the parameter range at low *ampR* and *ampE*.

The large parameter range that complies with all observational constraints indicates that the scenario in section 4.1 is far from unique in its ability to explain coeval variations in $^{87}Sr/^{86}Sr$ and salinity when forced by precession-driven climatic variations. However, in the default setup no scenarios have been found to comply with all constraints when precession-driven climatic changes are small. Whether the required relatively large changes in the fresh water budget are realistic will be discussed in section 5.1. In the next section, the sensitivity of the results to the choice of parameters in the default setup will be examined.

4.3. Sensitivity of the Results to Changes in the Default Setup

4.3.1. The Average Water Budget

In the previous section, the precession-averaged total Mediterranean river input, which is based on the reference Miocene water budget times *fR*, has been constant in all experiments. The *fR* values for both the deep and marginal basin have been kept at 1.5, a value based on the results of *Topper et al*. [2011] and *Topper and Meijer* [2013]. Even though 1.5 has given optimal results in previous studies, it is not the only possible value. To assess the sensitivity of the results to a different value for *fR* and the uniqueness of the results in the previous section, the model has been initiated with 256 different combinations of fR_D and fR_M, both in the range of 0.5–2.0.

The systematic variation of fR_D and fR_M could be visualized with 256 figures like Figure 4, one for each combination of the two parameters. However, we are mainly interested in changes in the size of the range that fits all constraints. For that reason, the percentage of the *ampR-ampE* range that fits all constraints is determined for every combination of g_{DA} and g_{MD} for all 256 combinations of fR_D and fR_M (Figure 5). For example, 73.3% of all *ampR-ampE* combinations fit all constraints at $g_{DA} = 10^2$ and $g_{MD} = 10^0$ in Figures 4i and 4j. This percentage is plotted at the corresponding g_{DA}-g_{MD} combination in Figure 5 at $fR_D = 1.5$ and $fR_M = 1.5$, i.e., within the black box. In the same way, percentages of the *ampR-ampE* range that fits all constraints are plotted for all fR_D-fR_M combinations in each of the 16 frames which represent distinct g_{DA}-g_{MD} combinations.

As shown in section 4.2, marginal basin water characteristics mimic those of the deep basin when $g_{MD} \geq 10^2$. This is visible again in Figure 5 where results are largely independent of fR_M at $g_{MD} \geq 10^2$. Moving from low to high fR_D, the first setting where all constraints are met occurs at or near $fR_D = 1.0$, the highest percentages are reached where $1.4 \leq fR_D \leq 1.7$, and percentages drop again toward higher fR_D.

Ignoring the influence of fR_M, an increase in fR_D causes a lowering of concentration and $^{87}Sr/^{86}Sr$ minima as well as maxima. At low fR_D, concentration minima are too high for any setting to comply with all constraints. From $fR_D \approx 1.0$ onward, $^{87}Sr/^{86}Sr$ and salinity minima reach their constraints at the same point where halite saturation ceases to be reached; first at high *ampR* and *ampE*, but with increasing fR_D this range expands toward lower amplitudes. Until $fR_D \approx 1.6$, gypsum saturation is reached in almost the whole *ampR-ampE* range. At even higher fR_D, minima are not limiting the range anymore. Gypsum and $^{87}Sr/^{86}Sr$ maxima become too low in an increasingly larger range toward higher fR_D. Consequently, the range that fits all constraints shrinks toward higher amplitudes and the percentages in Figure 5 decrease again. At $fR_D = 1.89$, the precession-averaged fresh water budget becomes positive and percentages drop further until none of the *ampR-ampE* ranges fit the constraints anymore (not shown).

At $g_{MD} = 10^0$, the influence of fR_M becomes apparent; percentages along a constant fR_D vary significantly with fR_M. The pattern of change and its cause are similar to that described for fR_D; percentages generally increase from low fR_M to an optimum around $fR_M = 1.0$ and drop toward higher fR_M. At low fR_M, the fresh water budget of the marginal basin is strongly negative, increasing the likelihood of halite saturation and high minima. At $fR_M = 0.95$, the marginal basin fresh water budget switches sign. Hence, maxima are harder to reach at higher fR_M.

The interaction between fR_D and fR_M can be advantageous for the range. When either a high fR_M lowers the minima where these were limiting the range ($fR_D \leq 1.5$) or a low fR_M heightens the maxima at high fR_D, the

© 2014. American Geophysical Union. All Rights Reserved.

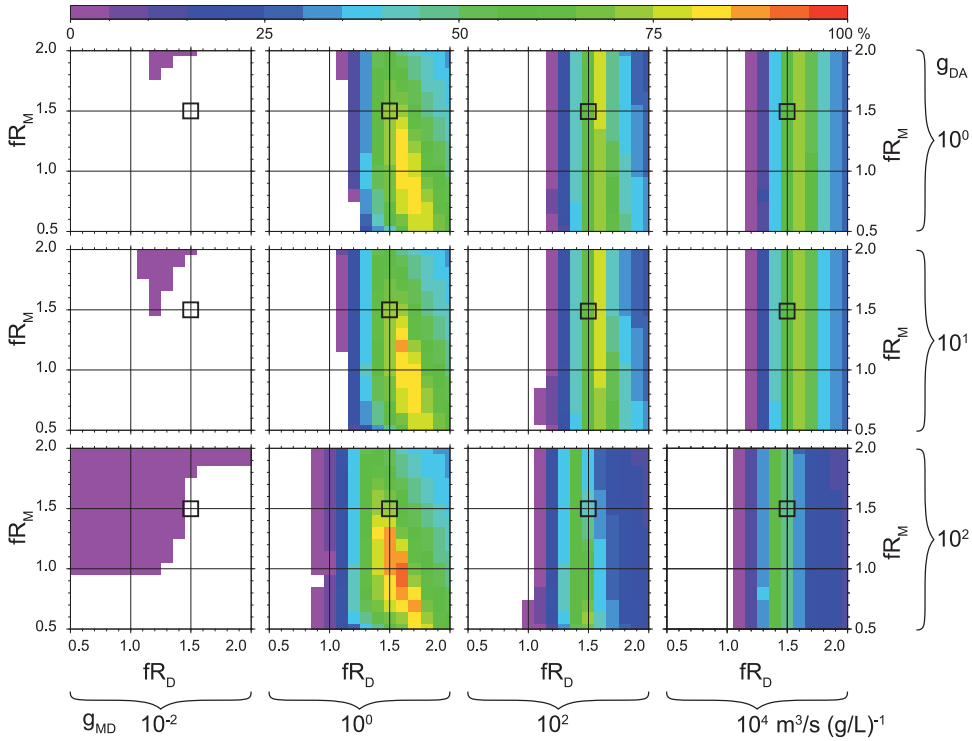

Figure 5. Sensitivity of the range that fits all constraints to changes in the precession-averaged river discharge of the marginal and deep basin. Shown is the percentage of the *ampR-ampE* range that fits all observational constraints for 256 models initiated with different combinations of fR_D and fR_M. The fR_M-fR_D combination that corresponds to the default setup from Figure 4 is indicated by the black box in each frame.

range increases. This strengthening effect, however, only plays an important role at $g_{MD} = 10^0$; at higher connectivity, the interbasinal exchange erases the influence of the marginal water budget, while at lower connectivity, the role of the deep basinal water budget is too limited.

At $g_{MD} = 10^{-2}$, a range that fits all constraints often exists at either extremely low or high *ampR* and *ampE*. Due to its relative independence of the deep basin, a marginal basin in this setting is hardly affected by fR_D. However, because halite saturation or gypsum undersaturation is prevailing and ranges that fit all constraints are insignificant and at extreme amplitudes, this setting cannot be considered a likely setting for PLG formation.

4.3.2. Riverine Strontium and Marginal Basin Characteristics

The riverine $^{87}Sr/^{86}Sr$ in the default setup is based on the present-day average value of the Nile and Rhone discharges which make up >80% of the total Mediterranean river input (Table 1). The riverine strontium concentration used in section 4.2 is only half the present-day values; present-day Sr concentrations are artificially elevated because the Nile has a reduced runoff and increased evaporation due to anthropogenic modifications, and the Rhone has been contaminated. Even though global ocean $^{87}Sr/^{86}Sr$ values are well known for the Late Miocene [e.g., *McArthur et al.*, 2001], riverine values are largely unknown. In the Late Miocene, river input was largely made up by North African rivers which nowadays run dry and did not drain the low $^{87}Sr/^{86}Sr$ basaltic rocks in the Nile catchment. A possible inflow from the Paratethys [*Krijgsman et al.*, 2010], with the low $^{87}Sr/^{86}Sr$ signature of the Volga [*Vasiliev et al.*, 2010], would have the same impact as a river and has therefore not been explicitly included. Moreover, on the marginal basin scale, the strontium characteristics of the river input will be strongly dependent on locally outcropping rocks in small catchments. Besides the basaltic rocks, relatively low $^{87}Sr/^{86}Sr$ comes from Mesozoic carbonates which outcrop over a vast area surrounding the Mediterranean [*Hartmann and Moosdorf*, 2012]. Groundwater, draining these carbonates, would affect the marginal basin in a similar fashion as river input and has also not been explicitly included in the model.

Given the uncertainties on both the riverine Sr concentration ($[Sr]_R$) and ratio, the experiments of section 4.2 have been repeated with riverine $^{87}Sr/^{86}Sr$ values within the Mesozoic ocean $^{87}Sr/^{86}Sr$ range, i.e.,

© 2014. American Geophysical Union. All Rights Reserved.

0.7065–0.7085, and riverine Sr concentrations of 150–450 $\times 10^{-6}$ kg m^{-3}, i.e., 50–150% of the present-day average concentration, to assess the sensitivity of the results to these parameters.

With respect to the results shown in Figure 4, only the $^{87}Sr/^{86}Sr$ minima and maxima are affected. Consequently, the parameter range that fits all constraints only changes if either the required $^{87}Sr/^{86}Sr$ maximum or minimum is not reached. With a low riverine $^{87}Sr/^{86}Sr$ (0.7065), the maximum $^{87}Sr/^{86}Sr$ constraint is reached at higher amplitudes compared to the default setup (0.7075). Nevertheless, the range that fits all constraints is largely unchanged at low riverine concentrations (150 $\times 10^{-6}$ kg m^{-3}), but shrinks rapidly when concentrations increase. With a high riverine $^{87}Sr/^{86}Sr$, on the contrary, a higher riverine concentration has a positive impact on the parameter range. In short, the largest amplitude range that meets all constraints occurs where riverine strontium characteristics are either a low $^{87}Sr/^{86}Sr_R$ (0.7065–0.7075) with a low $[Sr]_R$, or a relatively high $^{87}Sr/^{86}Sr_R$ (0.7085) with a high $[Sr]_R$.

Given the wide range of settings in which Messinian marginal basins formed, they cannot all be expected to have had a similar river input, volume, and surface area. To assess the sensitivity of the results to these basin characteristics, all three have been systematically varied in a series of experiments.

While river input, volume, and surface area have a clear influence on the water characteristics of the marginal basin, their influence is mainly in severely restricted settings. A larger volume and river input, compared to the default setup, lower the halite maxima and, hence, create a range that fits all constraints at $g_{MD} = 10^{-2}$. At higher connectivities, a larger volume and river input reduce the range that fits all constraints due to lower gypsum maxima. Judging from the model results only, the depth of the basin does not severely affect the results. In reality water chemistry presumably inhibited gypsum formation in deep(er) basins [*de Lange and Krijgsman*, 2010; *Lugli et al*., 2010]. For the size of the river input, a clear preference exists for twice the amount of river input per unit surface with respect to the Mediterranean average. A larger size (surface area and volume) does not significantly change the results if the connectivity changes proportionally.

A more extensive examination of the sensitivity of the results to riverine strontium characteristics, the size of the marginal basin, and its river input can be found in *Topper* [2013].

4.4. Duration of Gypsum Deposition

The cyclic alternations of shale/sapropel and gypsum layers in PLG deposits are evidence for periodic undersaturation of gypsum in the marginal basins. The duration of actual gypsum deposition, however, cannot be determined from the deposits since no high-resolution chronological constraints are available yet. In contrast, in the model, the number of years with gypsum saturation within a single precession cycle can be easily tracked. Figure 6a shows the duration of gypsum deposition in the same parameter space as Figure 4. Durations for the marginal basin are only shown where all observational constraints are met. For the deep basin all durations are shown, black lines indicate the ranges corresponding to different g_{DA}.

The range of parameters that fits all observational constraints is mainly restricted by the minimum salinity and maximum gypsum saturation constraints. Because of this, all scenarios where gypsum saturation in the marginal basin is never reached or continues throughout the whole precession cycle have already been excluded from the results in Figure 6a. All durations are in the range 1–8000 year.

At the end of the interval where R > E-P, minimum salinities are reached and salinities start to rise. If the connection with the Atlantic is relatively large ($g_{DA}=10^2$), the Mediterranean salinity rise is slow compared to more restricted settings. Hence, gypsum saturation is reached later and gypsum deposition only takes place in the last kyr(s) of the E-P > R interval. Because the E-P > R interval becomes longer toward higher amplitude variations, the duration of gypsum deposition increases concurrently from <1 kyr to 4–5 kyr ($g_{DA}=10^2$; Figure 6a).

When the connection with the Atlantic is severely restricted, the duration of gypsum deposition is relatively constant at 5–7 kyr ($g_{DA} \leq 10^1$ and $g_{MD} \geq 10^2$). In this range, the salinity rise in the deep basin is sufficiently fast when the fresh water budget becomes negative that the length of the E-P > R interval only plays a minor role. Furthermore, the length of the E-P > R interval changes mostly at low amplitude variations, i.e., the range that does not fit all constraints. The marginal basin water budget only becomes important when the exchange is severely restricted ($g_{MD} = 10^0$). Because the marginal basin has a precession-averaged

© 2014. American Geophysical Union. All Rights Reserved.

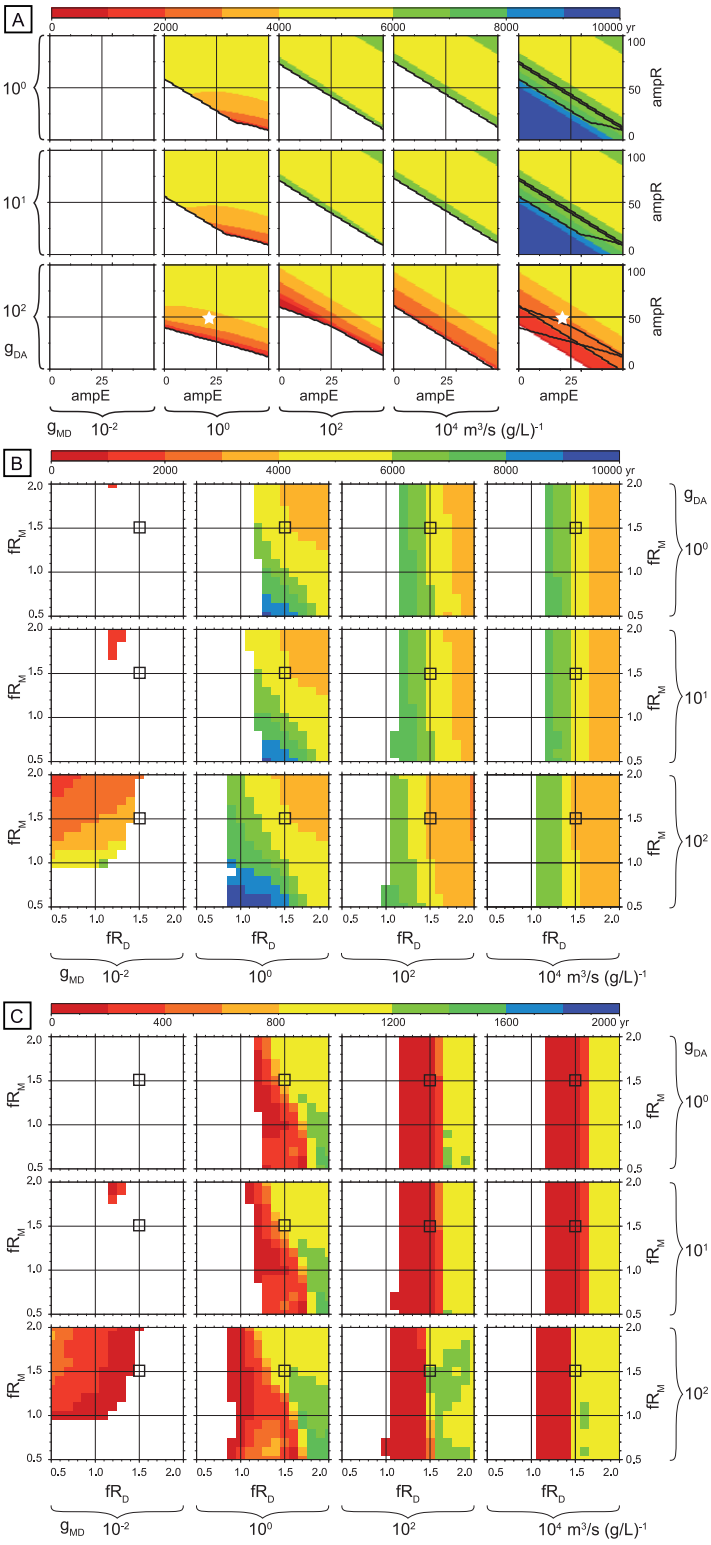

Figure 6. (a) The duration of gypsum deposition in marginal and deep basin. Durations for the marginal basin are only shown where all observational constraints are met. All durations are shown for the deep basin; the three black lines correspond to the ranges at different g_{DA}. The parameters along the axes are the same as in Figure 4. Figure 6b illustrates the sensitivity of the duration of gypsum deposition in the marginal basin to changes in the precession-averaged river discharge of the marginal basin. Plotted is the average duration of gypsum deposition in the *ampR-ampE* range that fits all observational constraints for 256 models initiated with different combinations of fR_D and fR_M. Figure 6c shows the corresponding standard deviation of the range of durations.

© 2014. American Geophysical Union. All Rights Reserved.

positive fresh water budget, the duration of gypsum saturation decreases significantly in a severely restricted marginal basin.

In Figure 6a, two other trends in the duration of gypsum deposition should be highlighted. With an increasing restriction of the Atlantic-Mediterranean connection, the duration of gypsum deposition increases in lower *ampR-ampE* settings. Hence, the thickness and volume of gypsum deposits formed in precession cycles with a lower amplitude are expected to increase when the Atlantic gateway becomes more restricted. Second, in a higher amplitude precession cycle thicknesses are expected to be larger as long as the Mediterranean is not severely restricted. However, because all other parameters, e.g., connectivity and basin size, have to be constant and the link between *ampR* and *ampE* and the amplitude of the precession signal is unknown, these correlations cannot be checked within the actual deposits.

For the results in Figure 6b, the duration of gypsum deposition has been calculated in the same range of fR_D and fR_M as used in Figure 5. Only the sensitivity to the *fR*s is examined here because all the parameters are examined in section 4.3. The average amount of river discharge in the deep and marginal basins has proven to affect gypsum concentration the most. Only looking at the ranges that fit all observational constraints, an average duration of gypsum formation in the marginal basin can be calculated for the whole *ampR-ampE* range of each g_{DA}-g_{MD} combination for all 256 combinations of fR_D and fR_M. To illustrate the range of durations in each *ampR-ampE* range, the standard deviation is shown in Figure 6b.

As a rather intuitive result, the duration of gypsum deposition decreases when the precession-averaged river input increases. A higher *fR*, either fR_D or fR_M, shortens the interval where E-P $>$ R. The influence of the marginal basin fresh water budget is more pronounced at lower g_{MD}, as in section 4.3.1, where exchange with the deep basin loses importance. The highest average duration ($\approx$10 kyr) is found at low *fR*s where the range that fits all constraints is small and located at high amplitudes. Nevertheless, in the *fR* range where percentages in Figure 5 are 75–100%, average durations can still go up to 8 kyr.

In the variation of the durations in the *ampR-ampE* range that fits all constraints, a clear division between high and low standard deviations is visible in each frame of Figure 6c. This division coincides with the switch in the limiting factor of the range that fits all constraints; at low *fR*s, these are the salinity and $^{87}Sr/^{86}Sr$ minimum, and at high *fR*s, the maximum gypsum concentration and $^{87}Sr/^{86}Sr$. Because reaching gypsum saturation is certain at low *fR*s and the range that meets all constraints is determined by salinity and $^{87}Sr/^{86}Sr$ minima, the *ampR-ampE* range with the lower durations is never in the range that complies with all constraints. At high *fR*s, gypsum saturation is not certain anymore, and the lower maximum gypsum concentrations make it the limiting factor. Therefore, shorter durations of gypsum deposition are included in the range that fits all constraints and hence standard deviations are higher.

5. Discussion

5.1. Precessional Variation of the Fresh Water Budget

The results in the previous sections have shown that $^{87}Sr/^{86}Sr$ and salinity variations in Mediterranean marginal basins can be driven by a precessional forcing. Riverine water characteristics (Sr concentration and ratio), basin features, and precession-average water budget all have a clearly identifiable impact on the size of the range of *ampR-ampE* combinations that meet all the observational constraints. The question remains whether the range of *ampR* and *ampE* is realistic.

In Figure 4, it is still clear what the lowest possible *ampR* and *ampE* are in the ranges that fit all constraints. For Figure 5, on the other hand, this information is lost due to the focus on the size of the range that fits all constraints. In Figure 7, the minimum *ampR* above which all constraints are met for different values of *ampE* is indicated for a series of experiments including those of Figure 5. For example, in Figure 5 at *ampR* = 6% at some combination of g_{DA}, g_{MD}, fR_D, and fR_M, all constraints are met when *ampE* $>$ 23%. To illustrate the sensitivity of this result to riverine strontium characteristics and marginal basin characteristics (see section 4.3.2), the experiments for Figure 5 have been repeated 5 times with $^{87}Sr/^{86}Sr_R = 0.7065$ (orange line) and 0.7085 (green), $[Sr]_R = 450 \times 10^{-6}$ kg m^{-3} (red), a larger river input in the marginal basin (purple), and a larger marginal basin volume (gray). In all these experiments, especially the high [Sr] *R* experiment, the minimum *ampR* and *ampE* needed to meet all constraints are higher compared to the default model setup. Changes are largest where riverine strontium characteristics are varied and smaller for

© 2014. American Geophysical Union. All Rights Reserved.

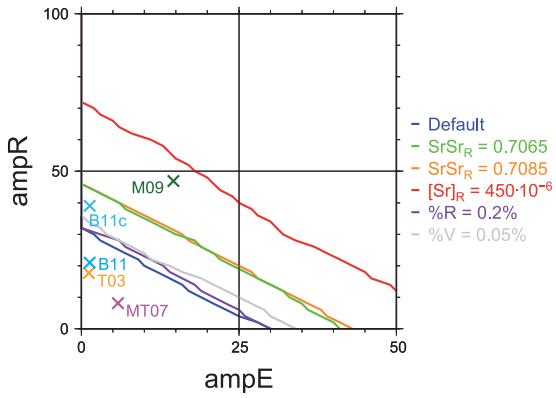

Figure 7. The minimum *ampR* and *ampE* above which scenarios exist that fit all observational constraints in Figure 5 (blue line). The other lines show the minimum *ampR* and *ampE* for experiments which differ from the default setup in only one parameter. Also indicated are the amplitudes of variation found in *Meijer and Tuenter* [2007] (MT07, purple cross), *Tuenter et al.* [2003] (T03, orange), *Bosmans et al.* [2012] (without/with Chad basin: B11/B11c, light blue), and *Murphy et al.* [2009] (M09, green).

changes in the marginal basin characteristics. However, in all experiments but the high $[Sr]_R$ experiment a combination of parameters exists where an *ampR* of 45% is able to reproduce all observations without any variation in E-P (*ampE* = 0 in Figure 7); the change in the fresh water budget due to the river input variation is large enough to reach both the required minima and maxima. Toward higher *ampE* a lower minimum *ampR* is needed.

Quantitative estimates of the variation of the fresh water budget of the Mediterranean are scarce. There are proxies for relative changes in the amount of river input and evaporation [e.g., *Köhler et al.*, 2010; *Vasiliev et al.*, 2013] which unfortunately cannot quantify the changes found. Currently, only climate models can give the required quantitative information.

The variation of precipitation, evaporation, and river discharge in the Mediterranean during a precession cycle has been studied by *Meijer and Tuenter* [2007] for the present-day climate and *Murphy* [2010] for the Late Miocene (Figure 7). The values for *ampR* and *ampE* from *Meijer and Tuenter* [2007] do not represent the maximum precession-driven change of R and E-P because the present-day situation, approximately a weak precession maximum, was compared with the strongest precession minimum of the last 1 Myr. When the results of the precession minimum and maximum experiments of *Tuenter et al.* [2003] (which provided the precession minimum data for *Meijer and Tuenter* [2007]) are used to calculate amplitudes of variation, *ampR* is significantly higher while *ampE* is lower. Moreover, the model used by *Tuenter et al.* [2003] is known to underestimate precipitation, and thus the amplitude of precessional variation of precipitation and runoff. Amplitudes calculated with a mid-Holocene and preindustrial run, i.e., a weak precession minimum and maximum, from a more recent climate model are already higher [*Bosmans et al.*, 2012]. Noteworthy is the large impact of the Chad basin, which was not draining into the Mediterranean in the model used by *Meijer and Tuenter* [2007] and *Tuenter et al.* [2003], on *ampR*. A repetition of the precession extrema experiments with other and/or more recent climate models is therefore expected to result in higher *ampR* and *ampE*.

The Miocene orbital forcing experiments of *Murphy* [2010] stand out owing to the higher *ampE* which is caused by a significant change in the precipitation over the Mediterranean due to changes in seasonal insolation. The *ampR* value is also significantly higher, with absolute discharges in the precession maximum below present-day values.

Even though the quality of the amplitude values from the climate models is hard to assess, it will do for an order of magnitude estimate. In the climate model results, *ampE* is consistently low compared to *ampR* values which also have a much larger spread. In our results, a range that fits all observational constraints can be found in the *ampE* range from climate models (1.2–14.6%) when *ampR* is at least 15–30% (Figure 7), well below the *ampR* of *Murphy* [2010]. Because these values represent the highest precession amplitude possible, *ampR* of precession cycles in lower eccentricity intervals will be lower. There, fortunately, remains a significant range between the *ampR* from the Late Miocene climate model and the minimum *ampR* we find to be needed to explain all variations during the PLG. Also, considering that the amplitudes found by *Tuenter et al.* [2003] are likely underestimated, we cautiously conclude that part of the amplitude ranges, mainly restricted by *ampE*, found required in this study is realistic.

5.2. The Setting for PLG Formation

Having systematically tested a large number of different settings for PLG formation in marginal basins, we can give a range of each of the parameters in which it is most likely that PLG formation took place:

© 2014. American Geophysical Union. All Rights Reserved.

1. In a large range of sizes of the Atlantic-Mediterranean and deep-marginal basin connections, an *ampR*-*ampE* range exists that fits all constraints from the deep and marginal basins ($10^0 \leq g_{DA} \leq 10^2$, $10^0 \leq g_{MD} \leq 10^4$). Only a severely restricted marginal basin ($g_{MD} = 10^{-2}$), i.e., with water characteristics as good as independent from those in the deep basin, is unlikely due to its tendency for either halite saturation and gypsum undersaturation. The largest range of parameters in all sensitivity experiments is usually reached where $g_{DA} = 10^2$, the least restrictive setting for Atlantic-Mediterranean exchange in our model results, and $g_{MD} = 10^0$, where the fresh water budget of the marginal and deep basin is equally important in determining the marginal basin water characteristics.

2. Riverine strontium characteristics should preferably be a combination of either a low $^{87}Sr/^{86}Sr_R$ (0.7065–0.7075) with a low $[Sr]_R$, or a relatively high $^{87}Sr/^{86}Sr_R$ (0.7085) with a high $[Sr]_R$. Rocks outcropping in the catchment areas draining into the Mediterranean comprise the whole range of $^{87}Sr/^{86}Sr$ values. Riverine [Sr] values vary significantly depending on the lithologies in the catchment, the season, and the river discharge [e.g., *Palmer and Edmond*, 1989]. The appropriateness of the range of [Sr], 0.5–1.5 times the present-day Mediterranean average riverine [Sr], is therefore hard to assess.

3. As long as the connectivity is proportional to the size of the basin, the size of the basin does not play a role in determining whether salinity and $^{87}Sr/^{86}Sr$ can fluctuate on a precessional timescale. A marginal basin deeper than 300 m, ignoring the fact that the depositional setting of gypsum is actually unlikely to be below 300 m [*Lugli et al*., 2010], reduces the likelihood of meeting all observational constraints. When river discharge in the marginal basin is 0.05–0.10% of the total Mediterranean river discharge, the marginal basin is most perceptible to $^{87}Sr/^{86}Sr$ and salinity fluctuations.

4. The preferred precession-averaged fresh water budget of the deep basin (fR_D) is in the range 1.4–1.7 times the default value, given by the Late Miocene water budget from *Gladstone et al*. [2007]. The marginal basin budget is of less importance as long as the marginal basin is not severely restricted. This range of deep basin *fR*s is significantly higher than the range in *Topper et al*. [2011] ($fR = 0.9$–1.3). The main cause for this difference is the interpretation of the $^{87}Sr/^{86}Sr$ data. In *Topper et al*. [2011], the lowest $^{87}Sr/^{86}Sr$ value in the PLG was taken to be the lowest value reached during the whole PLG interval, while we here assume that $^{87}Sr/^{86}Sr$ was likely to be lower during times of gypsum undersaturation. With a similar interpretation of the $^{87}Sr/^{86}Sr$ data, the range of *Topper et al*. [2011] shifts to a range of *fR*s similar to those found here. Another, but less influential, origin of the difference can be found in the precession-driven forcing which changes the average water characteristics with respect to those found with constant forcing.

5. The variability in the fresh water budget does not have to be large to allow for the observed salinity and $^{87}Sr/^{86}Sr$ range. The *ampR* can be as low as 23% when *ampE* is only 6%. Given the large range of *fR*s, basin size, and connectivities at which a realistic range of amplitudes can explain all observations of the PLG, the coeval salinity and $^{87}Sr/^{86}Sr$ variation in the Vena del Gesso basin is unlikely to be unique to this location. Similar variations in $^{87}Sr/^{86}Sr$ can probably be found in many, if not all, PLG deposits in marginal Mediterranean basins.

6. Conclusions

When data are as yet insufficient to verify or refute a hypothesis, modeling can be the way forward, as shown in this study. A simple box model setup to represent the Late Miocene Mediterranean contains the essential processes and parameters to assess whether precession-driven changes in the fresh water budget can drive $^{87}Sr/^{86}Sr$ and salinity fluctuations in Mediterranean marginal basins. With a specific set of parameters, a single model was run to demonstrate a proof of concept: $^{87}Sr/^{86}Sr$ and salinity fluctuations during the PLG can be driven by precession induced climate changes.

An extensive sensitivity study has shown that:

1. The connection between the Atlantic and Mediterranean has to be restricted during the PLG interval, while the connection between the deep and marginal Mediterranean basins can be anything from nonrestrictive to restrictive.

© 2014. American Geophysical Union. All Rights Reserved.

2. Within a realistic range for the Mediterranean, a preferred combination of riverine strontium characteristics, i.e., concentration and ratio, exists where concentration and ratio are either both high or both low.

3. A marginal basin can have a large range of sizes without affecting its likelihood of producing $^{87}Sr/^{86}Sr$ and salinity fluctuations as long as the connection with the deep basin is proportional to its size.

4. The precession-averaged fresh water budget of the Mediterranean is most suitable for coeval $^{87}Sr/^{86}Sr$ and salinity variations when river input is considerably more dominant than in the present-day situation. In this relatively "wet" setting, the amplitudes of R and E-P variations during a precession cycle are within the range of amplitudes derived from orbital extrema experiments with climate models.

The large range of parameters that produces the proposed coeval $^{87}Sr/^{86}Sr$ and salinity fluctuations in a marginal basin during the PLG indicates that these fluctuations are probably not restricted to the specific setting of the Vena del Gesso basin from which the most comprehensive $^{87}Sr/^{86}Sr$ data set derives. It is therefore likely that future sampling of other basins will find similar variations.

Acknowledgments
For constructive comments on the manuscript and useful discussions, we thank Rocco Gennari, Andrea Bergamasco, and Rinus Wortel. We are grateful to Joyce Bosmans and Erik Tuenter for providing us with their climate model results. Comments and suggestions from two reviewers, Wout Krijgsman and Bernhard Peucker-Ehrenbrink, have helped to improve this article. R.P.M.T. is supported by the Netherlands Research Center for Integrated Solid Earth Science. Computational resources for this work were also provided by ISES (ISES 3.2.5 High End Scientific Computation Resources). Figures in this paper were created using GMT version 4.5.1 [*Wessel and Smith*, 1991].

References

Albarède, F., and A. Michard (1987), Evidence for slowly changing $^{87}Sr/^{86}Sr$ in runoff from freshwater limestones of southern France, *Chem. Geol.*, *64*, 55–65.

Bosmans, J. H. C., S. S. Drijfhout, E. Tuenter, L. J. Lourens, F. J. Hilgen, and S. L. Weber (2012), Monsoonal response to mid-holocene orbital forcing in a high resolution GCM, *Clim. Past*, *8*, 723–740.

Brass, G. W. (1976), The variation of the marine $^{87}Sr/^{86}Sr$ ratio during Phanerozoic time: Interpretation using a flux model, *Geochim. Cosmochim. Acta*, *40*, 721–730.

Commission Internationale pour l'Exploration Scientifique de la Méditerranée (CIESM) (2008), *The Messinian Salinity Crisis from mega-deposits to microbiology—A consensus report, in* CIESM Workshop Monographs*, edited by F. Briand, No. 33*, pp. 168, CIESM, Monte-Carlo, Monaco.

de Lange, G., and W. Krijgsman (2010), A unifying mechanism for shallow gypsum and deep dolomite formation during the Messinian Salinity Crisis, *Mar. Geol.*, *275*, 273–277.

Flecker, R., S. de Villiers, and R. M. Ellam (2002), Modelling the effect of evaporation on the salinity-$^{87}Sr/^{86}Sr$ relationship in modern and ancient marginal-marine systems: The Mediterranean Messinian Salinity Crisis, *Earth Planet. Sci. Lett.*, *203*, 221–233.

Gladstone, R., R. Flecker, P. Valdes, D. Lunt, and P. Markwick (2007), The Mediterranean hydrologic budget from a Late Miocene global climate simulation, *Palaeogeogr. Palaeoclimatol. Palaeocol.*, *251*, 254–267.

Hartmann, J., and N. Moosdorf (2012), The new global lithological map database GLiM: A representation of rock properties at the Earth surface, *Geochem. Geophys. Geosyst.*, *13*, Q12004, doi:10.1029/2012GC004370.

Hilgen, F. J., W. Krijgsman, C. G. Langereis, L. J. Lourens, A. Santarelli, and W. J. Zachariasse (1995), Extending the astronomical (polarity) time scale into the Miocene, *Earth Planet. Sci. Lett*, *136*(3), 495–510.

Köhler, C. M., D. Heslop, W. Krijgsman, and M. J. Dekkers (2010), Late Miocene paleoenvironmental changes in North Africa and the Mediterranean recorded by geochemical proxies (Monte Gibliscemi section, Sicily), *Palaeogeogr. Palaeoclimatol. Palaeocol.*, *285*, 66–73.

Krijgsman, W., F. J. Hilgen, I. Raffi, F. J. Sierro, and D. S. Wilson (1999), Chronology, causes and progression of the Messinian Salinity Crisis, *Nature*, *400*, 652–655.

Krijgsman, W., M. Stoica, I. Vasiliev, and V. V. Popov (2010), Rise and fall of the Paratethys Sea during the Messinian Salinity Crisis, *Earth Planet. Sci. Lett.*, *290*, 193–191.

Kutzbach, J. E., X. Liu, and Z. Liu (2008), Simulation of the evolutionary response of global summer monsoons to orbital forcing over the past 280,000 years, *Clim. Dyn.*, *30*, 567–579.

Leeder, M. (1999), Sedimentology and Sedimentary Basins: From Turbulence to Tectonics, 592 pp., Blackwell Sci., Oxford, U. K.

Lugli, S., M. A. Bassetti, V. Manzi, M. Barbieri, A. Longinelli, and M. Roveri (2007), The Messinian 'Vena del Gesso' evaporites revisited: Characterization of isotopic composition and organic matter, *Geol. Soc. Spec. Publ.*, *285*, 179–190.

Lugli, S., V. Manzi, M. Roveri, and B. C. Schreiber (2010), The Primary Lower Gypsum in the Mediterranean: A new facies interpretation for the first stage of the Messinian salinity crisis, *Palaeogeogr. Palaeoclimatol. Palaeocol.*, *297*, 83–99.

Manzi, V., R. Gennari, S. Lugli, M. Roveri, N. Scafetti, and B. C. Schreiber (2012), High-frequency cyclicity in the Mediterranean Messinian evaporites: Evidence for solar-lunar climate forcing, *J. Sediment. Res.*, *82*(12), 991–1005.

Manzi, V., R. Gennari, F. Hilgen, W. Krijgsman, S. Lugli, M. Roveri, and F. J. Sierro (2013), Age refinement of the Messinian salinity crisis onset in the Meditteranean, *Terra Nova*, *25*, 315–322.

Mariotti, A., M. V. Struglia, N. Zeng, and K.-M. Lau (2002), The hydrological cycle in the Mediterranean region and implications for the water budget of the Mediterranean Sea, *J. Clim.*, *15*, 1674–1690.

McArthur, J. M., R. J. Howarth, and T. R. Bailey (2001), Strontium isotope stratigraphy: LOWESS version 3: Best fit to the marine Sr-isotope curve for 0–509 Ma and accompanying look-up table for deriving numerical age, *J. Geol.*, *109*, 155–170.

Meijer, P. Th., and W. Krijgsman (2005), A quantitative analysis of the desiccation and re-filling of the Mediterranean during the Messinian Salinity Crisis, *Earth Planet. Sci. Lett.*, *240*, 510–520.

Meijer, P. Th., and E. Tuenter (2007), The effect of precession-induced changes in the Mediterranean freshwater budget on circulation at shallow and intermediate depth, *J. Mar. Syst.*, *68*, 349–365.

Meijer, P. Th., R. Slingerland, and M. J. R. Wortel (2004), Tectonic control on past circulation of the Mediterranean Sea: A model study of the Late Miocen, *Paleoceanography*, *19*, PA1026.

Murphy, L. (2010), *The climate impact of the Messinian salinity crisis, PhD thesis*, Univ. of Maryland, College Park.

Murphy, L. N., D. B. Kirk-Davidoff, N. Mahowald, and B. L. Otto-Bliesner (2009), A numerical study of the climate response to lowered Mediterranean sea level during the Messinian Salinity Crisis, *Palaeogeogr. Palaeoclimatol. Palaeocol.*, *279*, 41–59.

 © 2014. American Geophysical Union. All Rights Reserved.

Palmer, M. R., and J. M. Edmond (1989), The strontium isotope budget of the modern ocean, *Earth Planet. Sci. Lett.*, *92*, 11–26.
Roveri, M., S. Lugli, V. Manzi, and B. C. Schreiber (2008), The Messinian Sicilian stratigraphy revisited: New insights for the Messinian salinity crisis, *Terra Nova*, *20*, 483–488.
Topper, R. P. M. (2013), *A model analysis of atypical marine sedimentation in mediterranean basins, PhD thesis*, Dep. of Earth Sci., Utrecht Univ., Utrecht, Netherlands.
Topper, R. P. M., and P. Th. Meijer (2013), A modelling perspective on spatial and temporal variations in Messinian evaporite deposits, *Mar. Geol.*, *336*, 44–60.
Topper, R. P. M., R. Flecker, P. Th. Meijer, and M. J. R. Wortel (2011), A box model of the Late Miocene Mediterranean Sea: Implications from combined $^{87}Sr/^{86}Sr$ and salinity data, *Paleoceanography*, *26*(3), PA3223.
Tuenter, E., S. L. Weber, and L. J. Lourens (2003), The response of the African summer monsoon to remote and local forcing due to precession and obliquity, *Global Planet. Change*, *36*(4), 219–235.
Tuenter, E., S. L. Weber, F. J. Hilgen, and L. J. Lourens (2005), Simulation of climate phase lags in response to precession and obliquity forcing and the role of vegetation, *Clim. Dyn.*, *24*, 279–295.
Vasiliev, I., G.-J. Reichart, G. R. Davies, W. Krijgsman, and M. Stoica (2010), Strontium isotope ratios of the Eastern Paratethys during the Mio–Pliocene transition; Implications for interbasinal connectivity, *Earth Planet. Sci. Lett.*, *292*, 123–131.
Vasiliev, I., G.-J. Reichart, and W. Krijgsman (2013), Impact of the Messinian Salinity Crisis on Black Sea hydrology—Insights from hydrogen isotopes analysis on biomarkers, *Earth Planet. Sci. Lett.*, *362*, 272–282.
Weber, S. L., and E. Tuenter (2011), The impact of varying ice sheets and greenhouse gases on the intensity and timing of boreal summer monsoons, *Quat. Sci. Rev.*, *30*(3–4), 469–479.
Wessel, P., and W. H. F. Smith (1991), Free software helps map and display data, *Eos Trans. AGU*, *72*(41), 441.

 © 2014. American Geophysical Union. All Rights Reserved.